

Highlights

1. Neuromuscular junction denervation is an early hallmark of KCC3-deleted mice
2. KCC3 does not contribute to motoneuron resting chloride handling
3. KCC3 is involved in motoneuron plateau potential during firing
4. KCC3 loss of function induces Na^+/K^+ ATPase $\alpha 1$ subunit mislocalization
5. Targeting electrical activity *in vivo* reduces neuromuscular junction denervation and restores Na^+/K^+ ATPase $\alpha 1$ membrane pattern in KCC3-deleted mice

KCC3 loss-of-function contributes to Andermann syndrome by inducing

activity-dependent neuromuscular junction defects

Melissa Bowerman^{1,2,3}, Céline Salsac¹, Véronique Bernard^{4,5,6}, Claire Soulard^{1,2}, Annie Dionne^{7,8}, Emmanuelle Coque^{1,2}, Salim Benlefk^{1,2}, Pascale Hince^{9,10}, Patrick A. Dion^{9,10}, Gillian Butler-Browne^{11,12,13}, William Camu^{1,14}, Jean-Pierre Bouchard^{7,8}, Eric Delpire¹⁵, Guy A. Rouleau⁹, Cédric Raoul^{1,2} and Frédérique Scamps^{1,2,*}

¹ The Institute for Neurosciences of Montpellier, Inserm UMR1051, Saint Eloi Hospital, Montpellier, France

² Université Montpellier 1&2, Montpellier, France

³ Present address: University of Oxford, Department of Physiology, Anatomy and Genetics, Oxford, UK

⁴ Université Pierre et Marie Curie UM CR 18, Paris, France

⁵ CNRS UMR8246, Paris, France

⁶ Inserm U1130, Paris, France

⁷ Université Laval, Québec, Canada

⁸ CHU de Québec, Hôpital de l'Enfant-Jésus, Département des sciences neurologiques, Québec, Québec, Canada

⁹ Montreal Neurological Institute and Hospital, Department of Neurology and Neurosurgery, McGill University, Montreal, Québec, Canada

¹⁰ Department of Pathology and Cellular Biology, Université de Montréal, Montréal, Québec, Canada

¹¹ UM76, Institut de Myologie, Université Pierre et Marie Curie, Paris, France

¹² U974, Inserm, Paris, France

¹³ UMR7215, CNRS, GH Pitié Salpêtrière, Paris, France

¹⁴ Department of Neurology, ALS Reference Center, Gui-de-Chauliac Hospital, Montpellier, France

¹⁵ Vanderbilt University Medical Center, Vanderbilt, USA

* To whom correspondence should be addressed:

Frédérique Scamps

The Neuroscience Institute of Montpellier

Inserm UMR1051, Saint Eloi Hospital

80 rue Augustin Fliche

34091 Montpellier cedex 05

France

Tel: +33499636033

Fax: +33499636020

e-mail: frederique.scamps@inserm.fr

Abstract

Loss-of-function mutations in the potassium-chloride cotransporter KCC3 lead to Andermann syndrome, a severe sensorimotor neuropathy characterized by areflexia, amyotrophy and locomotor abnormalities. The molecular events responsible for axonal loss remain poorly understood. Here, we establish that global or neuron-specific KCC3 loss-of-function in mice leads to early neuromuscular junction (NMJ) abnormalities and muscular atrophy that are consistent with the pre-synaptic neurotransmission defects observed in patients. KCC3 depletion does not modify chloride handling, but promotes an abnormal electrical activity among primary motoneurons and mislocalization of Na⁺/K⁺-ATPase α 1 in spinal cord motoneurons. Moreover, the activity-targeting drug carbamazepine restores Na⁺/K⁺-ATPase α 1 localization and reduces NMJ denervation in *Slc12a6*^{-/-} mice. We here propose that abnormal motoneuron electrical activity contributes to the peripheral neuropathy observed in Andermann syndrome.

Keywords

Motoneuron, Andermann syndrome, chloride homeostasis, electrical activity, neuromuscular junction, Na⁺/K⁺ ATPase

Highlights

1. Neuromuscular junction denervation is an early hallmark of KCC3-deleted mice
2. KCC3 does not contribute to motoneuron resting chloride handling
3. KCC3 is involved in motoneuron plateau potential during firing
4. KCC3 loss of function induces Na⁺/K⁺ ATPase α 1 subunit mislocalization
5. Targeting electrical activity *in vivo* reduces neuromuscular junction denervation and restores Na⁺/K⁺ ATPase α 1 membrane pattern in KCC3-deleted mice

Introduction

Andermann syndrome is an autosomal recessive neurodevelopmental and neurodegenerative disorder characterized by peripheral neuropathy with variable agenesis of the corpus callosum (ACCPN) (Larbrisseau et al., 1984; Mathieu et al., 1990), hypotonia and amyotrophy (DeBraekeleer et al., 1993) and is caused by mutations within the cation-chloride cotransporter KCC3 (Howard et al., 2002).

KCC3-deficient mice reproduce the typical ACCPN sensorimotor histopathology, displaying impaired locomotor and sensorimotor gating capacities and decreased peripheral nerve conduction (Howard et al., 2002; Boettger et al., 2003; Sun et al., 2010; Shekarabi et al., 2012). Axonal swelling, neurodegeneration and hypomyelination of the sciatic nerve seem to account for the peripheral neuropathy. Both enveloping glial cells and demyelinating events have been proposed as the primary events responsible for reduced nerve conduction and neurodegeneration in mice and patients (Howard et al., 2002; Dupre et al., 2003; Sun et al., 2010). However, neuron-specific KCC3 deletion in mice is sufficient to induce peripheral neuropathy, supporting a neuronal-dependent neuropathy (Shekarabi et al., 2012)

KCC3 belongs to the family of cation-chloride cotransporters coded by the *Slc12a* genes (Mount et al., 1999). The *Slc12a* gene family comprises seven members coding for two inwardly directed $\text{Na}^+\text{-K}^+\text{-2Cl}^-$ cotransporters (*Slc12a2* for ubiquitous NKCC1 and *Slc12a1* for kidney specific NKCC2), one $\text{Na}^+\text{-Cl}^-$ cotransporter (*Slc12a3* for kidney specific NCC) and four outwardly directed $\text{K}^+\text{-Cl}^-$ cotransporters, (*Slc12a4-7* for KCC1-4, respectively) (Gagnon and Delpire, 2013). These membrane proteins are responsible for a wide variety of functions including cell volume regulation (O'Neill, 1999) and maintenance of intracellular chloride concentration $[\text{Cl}^-]_i$ (Blaesse et al., 2009). Following an osmotic challenge, KCCs

extrude K^+ and Cl^- ions together with water. Concordantly, axon swelling and periaxonal fluid accumulation are observed early in postnatal day (P)3, P8 and P30 KCC3-depleted (*Slc12a6*^{-/-}) mice followed by axonal loss in 7-8 month old adult mice (Byun and Delpire, 2007). As younger P30 mice perform poorly motor tests without any apparent axonal degeneration, it is assumed that defects in volume regulation are major contributor to impaired motor and balance functions (Howard et al., 2002; Byun and Delpire, 2007). However, the potential impact of KCC3 loss-of-function on neuromuscular junction (NMJ) integrity, which could also account for early motor defects, has never been explored, nor have activity-dependent effects of KCC3 through its potential control on neuronal intracellular Cl^- and K^+ content (Boettger et al., 2003; Lucas et al., 2012).

Here, we show that axon denervation occurs at the NMJ in P30 *Slc12a6*^{-/-} mice, therefore representing an early sign of the peripheral neuropathy. We further demonstrate that KCC3 loss-of-function does not modify the developmental chloride shift observed in spinal cord and isolated motoneurons. Instead, *Slc12a6*^{-/-} motoneurons display an abnormal electrical activity, a possible consequence of an unbalanced ionic homeostasis during firing behaviour related to Na^+/K^+ -ATPase dysfunction. Consistent with this proposed detrimental role on electrical activity, we found that a pharmacological decrease of motoneuron activity *in vivo* ameliorated NMJ innervation of *Slc12a6*^{-/-} mice. Combined with the functional analysis of nerve-evoked muscle contraction in ACCPN patients, our results highlight pre-synaptic-dependent defects as playing a central part of the Andermann syndrome and identify a novel mechanism by which loss of KCC3 leads to motor symptoms in this neurodevelopmental disorder.

Material and methods

Animals

All animal experiments were approved by the national ethics committee on animal experimentation, and were done in compliance with the European community and national directives for the care and use of laboratory animals. *Slc12a6*^{+/-} mice, described in (Howard et al., 2002) were maintained on a C57BL/6 background and we used the offspring of crosses between heterozygotes. For experiments using *nsSlc12a*^{Δ18/Δ18} mice, described in (Shekarabi et al., 2012), we used tissues collected at McGill University.

For *in vivo* experiments, carbamazepine (CBZ) or vehicle was administered to P10 *Slc12a6*^{-/-} mice by intraperitoneal injection of 0.025 mg/g/day for 20 consecutive days as described in (Li et al., 2013). P30 mice were then euthanized and muscles processed for neuromuscular junction analysis. A stock solution was prepared at 2.5 mg/ml using 12.5 mg CBZ (Santa-Cruz Biotechnology) diluted with 5 ml 2-Hydroxypropyl-β-cyclodextrin (Santa-Cruz Biotechnology) and stored at +4°C.

Motoneuron culture

Genotyping was carried out by PCR on tail DNA of E12.5 embryos obtained from *Slc12a6*^{+/-} mice breeding. Embryos were kept at 4°C in Hibernate-E medium (Life technologies) during the course of genotyping. Afterwards, *Slc12a6*^{+/+} and *Slc12a6*^{-/-} embryos were processed for cultures as described previously (Raoul et al., 2002). Briefly, cells were dissociated mechanically after trypsin treatment of the dissected spinal cords. The largest cells were isolated using iodixanol density gradient purification. To get highly purified motoneuron cultures, we added an immunopurification step using magnetic cell sorting technology (Arce et al., 1999). In experiments using *Hb9::GFP* embryos to identify motoneurons, we found that this protocol yielded roughly 80-90% of GFP-positive neurons. Briefly, isolated neurons were incubated at +4°C in 80 μl L-15 medium containing 0.5% bovine serum albumin (BSA) and 2 μl of an anti-mouse p75 monoclonal antibody (Millipore) for 20 minutes, followed, after wash-out, by a 15 minute incubation in 80 μl L-15, 0.5% BSA, 10 μl goat anti-mouse IgG

microbeads. The magnetically labeled cells were applied onto a separation column and retained using a magnet (Miltenyi Biotec). Following wash-out of the p75 negative fraction with L-15, 05% BSA, cell sorting was achieved by removing the magnet. After a final BSA cushion, motoneurons were plated onto poly-ornithine laminin-coated wells in Neurobasal (Life Technologies) medium containing 2% horse serum, 2% B-27 supplement (Life Technologies), 50 μ M L-glutamine, 25 μ M L-glutamate, 25 μ M β -mercaptoethanol and a cocktail of neurotrophic factors (1 ng/ml BDNF, 100 pg/ml GDNF, and 10 ng/ml CNTF).

Electrophysiological recordings

For chloride reversal potential determination of 1 and 7 *days in vitro* (DIV) motoneurons, chloride GABA_A current was recorded at 20-22°C with the gramicidin-perforated patch-clamp technique using an Axopatch 200B amplifier (Dipsi Industrie). The bathing solution contained 140 mM TEA-Cl, 3.5 mM MgCl₂, 10 mM glucose and 10 mM HEPES, adjusted to pH 7.4 with CsOH, and the pipette solution contained 140 mM CsCl, 1.5 mM Mg-ATP, 0.5 mM Na-GTP, 0.1 mM EGTA and 10 mM HEPES, adjusted to pH 7.35. We determined $[Cl^-]_i$, by adding 50 μ g/ml gramicidin A (Sigma-Aldrich) to the pipette solution as described in (Pieraut et al., 2007). $[Cl^-]_i$ was calculated according to the Nernst equation: $E_{rev} = RT/ZF \times (\log ([Cl^-]_i / [Cl^-]_e))$, where $RT/ZF = 58$ mV at room temperature and $[Cl^-]_e = 147$ mM.

For electrical activity measurements, 7-8 DIV motoneurons from *Slc12a6*^{+/+} and *Slc12a6*^{-/-} were recorded under whole-cell patch clamp at room temperature in a bathing solution containing 140 mM NaCl, 5 mM KCl, 2 mM CaCl₂, 1.5 mM MgCl₂, 10 mM glucose and 10 mM HEPES, adjusted to pH 7.35. The patch pipette contained 10 mM KCl, 135 mM K-methane-sulfonate, 1.5 mM Mg-ATP, 0.5 mM Na-GTP, 0.1 mM EGTA and 10 mM HEPES, adjusted to pH 7.35. Spontaneous activity of motoneurons was recorded with the loose-patch technique after forming a 30-50 M Ω contact between cell membrane and recording electrode. The electrode was filled with the extracellular solution. Ouabain, apamin and cadmium

chloride were from Sigma.

RNA extraction and RT-qPCR

For primary cultures, total mRNA was extracted from roughly 30000 purified embryonic motoneurons at 1 or 7 DIV with the RNeasy Mini Kit (Qiagen). For E12.5, P1 and P30 lumbar spinal cords, the tissues were harvested in ~~RNA~~ stabilization buffer (Qiagen). Lysis buffer was used for pestle tissue crushing and homogenization by passing the lysate through needles. Lysates were then mixed with an equal volume of 70% ethanol, and total mRNA was separated from other cellular components on RNeasy minispin columns. The eluted mRNA was quantified by spectrophotometry (Nanodrop). Following gDNA wipe out, reverse transcription (RT) was performed with 100 ng to 1 µg of mRNA with the Quantitect RT kit (Qiagen). The collected cDNA was diluted to 50 ng (culture) or 100 ng (tissue) with water and stored at -20°C until further use. Primers were designed with Primers 3.0 software. The sequences of the primers used are published in (Lucas et al., 2012). Quantitative PCR was performed on 5 or 10 ng cDNA with SYBR Green (Qiagen) for detection and the LightCycler system (Roche Diagnostics). After initial activation for 15 min at 95°C, 45 cycles of 94°C for 15 s, 60°C for 20 s and 72°C for 35 s were carried out. After PCR amplification, a melting curve analysis was carried out to check that the PCR was specific. Polymerase (RNA) II polypeptide J (*Polr2J*) level was used to normalize the amounts of cDNA. ΔC_t was calculated as the difference between the C_t values, determined with the equation $2^{-\Delta C_t}$.

Immunohistochemistry.

For spinal cord immunohistochemistry, 4-week-old mice were anaesthetized and perfused transcardially with 4% paraformaldehyde. Lumbar spinal cords were removed and post-fixed in 4% paraformaldehyde, flash-frozen and cut at a 12µm thickness. For Na⁺/K⁺-ATPase α1 immunohistochemistry, a citrate buffer antigen retrieval step was performed. The sections were then rinsed 5 minutes in PBS and incubated for 2 hours at room temperature in blocking

solution (TBLS (10% NaN₃), 20% goat serum, 0.3% Triton X-100). This was followed by an overnight incubation at +4°C with the primary antibodies. Subsequently, sections were incubated 1 hour with secondary antibodies and mounted in Mowiol.

For neuromuscular junction immunohistochemistry, *tibialis anterior* (TA) muscle sections were labeled by immunohistochemistry to allow quantification of neuromuscular innervation and endplate morphology as described previously (Bowerman et al., 2012). For ubiquitous *Slc12a6*^{-/-} mice, whole TA muscles were dissected from 4-week-old animals and fixed in 4% paraformaldehyde for 15 minutes. Following the removal of connective tissue, the TA muscles were incubated with α -bungarotoxin Alexa Fluor 555 conjugate (α BTX)(Life Technologies; 1:1000) for 20 minutes at room temperature. The TA muscles were then incubated in methanol at -20°C for 5 minutes, followed by an overnight incubation at +4°C with the SV2 and neurofilament antibodies. Incubation with the secondary antibodies was performed the following day at room temperature for 1 hour. Finally, two to three thin filets per stained TA were cut and mounted in Mowiol. All filets were single sections of the surface of the TA muscle.

For neuron-specific *Slc12a6* deletion (*nsSlc12a6* ^{$\Delta 18/\Delta 18$}) mice, NMJ analysis was performed on longitudinal frozen sections of 8-week-old animals. TAs were post-fixed in 4% paraformaldehyde, flash-frozen and cut at a 10 μ m thickness. The sections were then rinsed 5 minutes in PBS and incubated for 2 hours at room temperature in blocking solution (TBLS (10% NaN₃), 20% goat serum, 0.3% Triton X-100). This was followed by an overnight incubation at 4°C with the primary antibodies. Subsequently, sections were incubated 1 hour with the secondary antibodies and the α BTX. All washes were done with PBS.

The primary antibodies used were: goat anti-choline acetyl transferase (ChAT)(1:250; AB144P; Millipore), mouse anti-Na⁺/K⁺-ATPase $\alpha 1$ (1:100; DSHB), mouse anti-2H3 (Neurofilament 165 kDa) (1:250; Developmental Studies Hybridoma Bank), mouse anti-SV2

(1:100; Developmental Studies Hybridoma Bank), mouse anti-SMI32 (1:1000; Sternberger Monoclonals). The secondary antibodies (Life Technologies) were used at 1:1000.

Images were taken with a Zeiss confocal microscope. Area of NMJs was determined using Image J software (National Institutes of Health, USA).

Electron microscopy

TA muscles collected from 4-week-old mice were fixed in a 2% paraformaldehyde/ 0.2% glutaraldehyde (Sigma-Aldrich) solution in PBS for 2 hours at 4°C. Samples were post-fixed overnight at +4°C in 2% PFA and rinsed in PBS. Bundles of about 20 muscle fibers were teased out and treated free-floating in solution. Muscle fibers were processed for electron microscopy as follows: junctions were identified by detecting nicotinic AChRs with α -bungarotoxin coupled to biotin (α BTX-biot) using a pre-embedding immunogold method. Muscle fibers were incubated in α BTX-biot (10 μ g/ml PBS) overnight at 20 °C. After washing, muscles were incubated in streptavidin coupled to gold particles (0.8 nm in diameter; Nanoprobes; 1:100 in PBS/BSA). The fibers were then washed and post-fixed in 1% glutaraldehyde. After washing in acetate buffer (0.1 M, pH 7), the signal of the gold immunoparticles was increased using a silver enhancement kit (HQ silver; Nanoprobes) for 3 minutes at room temperature in the dark. Finally, after washing in acetate buffer, sections were treated with 1% osmium, dehydrated and embedded in resin. Ultrathin sections were cut, stained with lead citrate and examined in a Philips CM120 transmission electron microscope (Eindhoven) equipped with a camera (Morada, Soft Imaging System, Olympus).

Hematoxylin and eosin staining of tibialis anterior sections

Whole tibialis anterior (TA) were dissected and placed overnight in 4% paraformaldehyde, then transferred to 70% ethanol solution. Tissues were embedded in paraffin, cut at a thickness of 5 μ m, deparaffinized and stained for hematoxylin and eosin. Images were acquired with a Leica DMRB. Muscle fiber area was measured using Image J software.

Compound muscle action potential recordings

Subjects were studied with a MEDTRONIC electromyography system (Natus Medical Inc.) at CHU de Québec. For ACCPN patients, repetitive nerve stimulations were performed for 3 different nerves. The spinal accessory nerve was recorded at the *trapezius* muscle, the facial nerve was recorded at the *nasalis* and the ulnar nerve was recorded at the *abductor digiti minimi*. Studies were performed using constant-current stimulation and a square-wave pulse of 0.2 ms duration delivered through a hand-held surface-stimulating electrode (13L36; Alpine Biomed) at the frequency of 3Hz. Filters were set at 3 Hz to 5 kHz. A decrement of more than 10% between the first and 4th compound muscle action potential (CMAP) was considered significant for a neuromuscular transmission defect.

Statistics

Data are presented as means \pm standard error of the mean (SEM). Data were analyzed by Mann-Whitney test for small samples, unpaired two-tailed Student's *t*-test, Fisher's exact test or analysis of variance (ANOVA).

Results

Loss of KCC3 results in aberrant pre-synaptic neuromuscular junction terminals

To investigate the early cellular and molecular mechanisms contributing to neurodegeneration in *Slc12a6*^{-/-} mice, we used P30 mice, as at this age axonal loss is not yet observed while impaired motor function can already be detected (Howard et al., 2002; Byun and Delpire, 2007). We found that both *Slc12a6*^{+/+} and *Slc12a6*^{-/-} mice displayed the same number of motoneurons within the lumbar spinal cord (Fig. 1A, B). However, analysis of NMJs within the *tibialis anterior* (TA) shows that *Slc12a6*^{-/-} mice display a significant increase in incompletely innervated NMJs compared to *Slc12a6*^{+/+} littermates (Fig. 1C, D). Imaging of wildtype and mutant TAs by electron microscopy (EM) revealed that approximately 40% of pre-synaptic NMJ terminals were abnormal, displaying a decreased terminal area associated with a large number of partially denervated endplates (Fig. 1E upper right, 1F) where, in some cases, the nerve is barely detectable (Fig. 1E lower panels, 1G). Indeed, in the latter event, terminal Schwann cell processes completely fill the pre-synaptic area (see asterix in Fig. 1E lower right). Thus, our data reveal that KCC3-depleted mice display early axonal defects at the NMJ that are not attributable to motoneuron death.

Neuronal-specific KCC3 deletion results in muscle atrophy and aberrant post-synaptic neuromuscular junction terminals

The loss of innervation led us to investigate the post-synaptic compartment of the NMJ. We observed that *Slc12a6*^{-/-} mice display significantly more morphologically immature endplates than *Slc12a6*^{+/+} littermates (Fig. 2A, B). To address whether these post-synaptic

abnormalities were due to KCC3-dependent intrinsic defects within muscle, we analyzed a mouse model with a neuron-specific deletion of *Slc12a6* exon 18 (*nsSlc12a6* ^{$\Delta 18/\Delta 18$}) that reproduces the peripheral neuropathy observed in ACCPN patients (Dupre et al., 2003; Shekarabi et al., 2012). Similarly to the ubiquitous *Slc12a6*^{-/-} mice, we find that post-synaptic terminals of 8-week old *nsSlc12a6* ^{$\Delta 18/\Delta 18$} display more disorganized morphology than wildtype littermates (Fig. 2C). Seeing as our results highlight aberrancies at the interface between nerve and skeletal muscle, we set out to determine the impact of loss of KCC3 on skeletal muscle parameters. Analysis of TA cross-sections reveals a reduction in myofiber area in *Slc12a6*^{-/-} mice (Fig. 2D, E) as well as in *nsSlc12a6* ^{$\Delta 18/\Delta 18$} mice compared to their respective *Slc12a6*^{+/+} littermates (Fig. 2F, G). Altogether these data support that a neuronal-specific role for KCC3 is most likely sufficient for endplate disorganization and amyotrophy.

Patients with Andermann syndrome do not display neuromuscular transmission defects

We next sought to support our observations of pre- and post-synaptic NMJ defects in ACCPN patients by assessing neuromuscular transmission using measurements of the muscle compound potential amplitude. Indeed, recordings of muscle compound action potential, CAP, amplitude allows the analysis of denervation-induced amyotrophy which typically leads to an overall decrease in CAP amplitude, but not in synaptic gain, therefore keeping a constant amplitude during repetitive nerve stimulation. Unlike denervation, end-plate defects induce progressive loss of synaptic transmission mirrored by a progressive decrease in CAP amplitude. Healthy individuals did not show any muscle fatigability during repetitive motor nerve stimulation (Fig. 3A). Patients with myasthenia gravis, a post-synaptic NMJ disorder due to the decrease of acetylcholine receptors, showed a gradual reduction of electrical muscle response attributed to decreased synaptic integration (Berrih-Aknin et al., 2014)(Fig. 3B). Consistent with our results obtained in murine models of Andermann syndrome, a strong

muscle weakness was also evident in ACCPN patients without signs of muscle fatigability under repetitive electrical stimulation (Fig. 3C). Altogether, our data support that presynaptic denervation due to loss of neuronal KCC3 contributes to amyotrophy in ACCPN patients.

Developmental expression of cation-chloride cotransporters in spinal cord is unaffected by KCC3 loss of function.

Having uncovered that defective pre-synaptic NMJ terminals occur early in *Slc12a6*^{-/-} mice, we next set out to determine how loss of KCC3 within motoneurons could lead to this aberrant synaptic maintenance. As Andermann syndrome is a neurodevelopmental disease, we first assessed the pattern of KCC3 expression during spinal cord development. Using quantitative PCR (qPCR), we show that KCC3 transcript is expressed as early as embryonic day 12.5 (E12.5) and its expression significantly increases during development (P30 compared to E12.5) (Fig. 4A). KCC3 exists as two distinct isoforms designated as KCC3a and KCC3b, with the latter isoform being renal-specific (Hiki et al., 1999; Mount et al., 1999; Race et al., 1999). Moreover, an exon 2-deleted form of KCC3a is preferentially expressed in the nervous system (Mercado et al., 2005; Le Rouzic et al., 2006; Lucas et al., 2012). We thus performed an RT-PCR to compare the expression of KCC3a isoforms in adult spinal cord and skeletal muscle. When using a primer set spanning exons 1 and 3 of KCC3a, the alternative splicing event was observed in both adult spinal cord and muscle, resulting in bands representing both the full-length (FL) and exon-deleted ($\Delta 2$) isoforms (Fig. 4B). However, the amount of exon 2-deleted transcript was clearly greater in spinal cord than in muscle. Using purified cultured motoneurons, we further confirmed the preferential expression of exon 2-deleted isoform in neuronal cells (Fig. 4B). Indeed, using pan-primers designed to span exons 13-15 (KCC3ab), we observed a single band, supporting the neuronal specificity of the exon

2-deleted KCC3a isoform. There was no detectable transcript with primers specific for KCC3b, consistent with its non-neuronal expression.

To determine whether KCC3 loss-of-function affects the chloride shift that occurs during development, we firstly assessed whether the expression of KCC2 and NKCC1 transcripts, the main cation-chloride cotransporters involved in $[Cl^-]_i$ maintenance, was modified in the spinal cord of *Slc12a6*^{-/-} mice. We compared transcript levels from E12.5, P1 and P30 mice and normalized P1 and P30 transcript levels to E12.5 values since KCC2 and NKCC1 transcript levels were not significantly different between groups at E12.5 (data not shown). Moreover, it was demonstrated that at E12.5 the chloride switch is not yet established in spinal motoneurons (Allain et al., 2011). Analysis of KCC2 transcript during development of *Slc12a6*^{+/+} spinal cord shows the molecular chloride shift signature of an increased expression of KCC2 (Rivera et al., 1999) between E12.5 and P1 (Fig. 4C). Further, we find that the expression of KCC2 transcript is not significantly different between *Slc12a6*^{+/+} and *Slc12a6*^{-/-} mice spinal cords at any time point. More surprisingly, we did not observe the expected decrease in the expression of NKCC1 transcript with maturation of *Slc12a6*^{+/+} spinal cord, but rather a roughly two-fold increase at P30 (Fig. 4D). Importantly, while NKCC1 levels are similar between *Slc12a6*^{+/+} and *Slc12a6*^{-/-} mice at E12.5 and P1, there is a further increase of NKCC1 transcript in P30 mutant mice compared to aged-matched controls. Seeing as NKCC1 plays an opposing role to that of KCC3 (inward chloride transport instead of outward), the increased expression of NKCC1 in KCC3-depleted mice may simply result from a non-specific compensatory mechanism or, alternatively, stem from other non-neuronal cell types within the spinal cord (Hubner et al., 2001; Yan et al., 2001). Nevertheless, we have identified on one hand a developmental increased transcript expression of all three cation-chloride cotransporters (KCC3, KCC2, NKCC1) in the spinal cord and on the other hand, an abnormal expression of NKCC1 in the spinal cord of P30 *Slc12a6*^{-/-} mice.

Developmental chloride shift in primary motoneuron cultures is unaffected by KCC3 loss-of-function

Since the spinal cord is a heterogeneous mixture of cells, we set out to functionally assess the impact of KCC3 loss-of-function on $[Cl^-]_i$ maintenance in primary cultures of purified motoneurons. To isolate motoneurons, we performed primary culture from E12.5 embryos, before the first wave of programmed death (Raoul et al., 1999) which allows the generation of enough material for combined molecular analyses and electrophysiological measurements. We first investigated the effect of KCC3 depletion on KCC2 and NKCC1 transcript expression during *in vitro* maturation of motoneurons isolated from E12.5 embryos between 1 and 7 days in vitro (DIV) (Fig. 4E). Our qPCR analysis reveals that NKCC1 transcripts are decreased while KCC2 transcripts are increased during normal maturation of *Slc12a6*^{+/+} motoneurons. In 7 DIV *Slc12a6*^{-/-} motoneurons, NKCC1 and KCC2 followed the same expression profiles than *Slc12a6*^{+/+} motoneurons, albeit with a significant reduction in the temporal increase of KCC2 transcript compared to control cells. Interestingly, the *in vitro* expression changes observed in motoneuron cation-chloride cotransporters between 1 and 7 DIV are qualitatively similar to those between E12.5 and P1 spinal cord (Fig. 4C, D).

The increase in KCC2 transcript together with the decrease in NKCC1 transcript observed between 1 and 7 DIV suggest that a chloride shift probably occurs during the maturation of cultured motoneurons. We therefore recorded the chloride reversal potential of GABA current (E_{GABA-A}) with the gramicidin-perforated patch-clamp method to determine if loss of KCC3 would influence chloride balance in motoneurons (Fig. 4F, G). Consistent with the temporal differential expression of KCC2 and NKCC1 transcripts in motoneurons, E_{GABA-A} showed a 22 mV hyperpolarization from -56 ± 3 mV ($n = 12$) at 1 DIV to -78 ± 3 mV ($n =$

10) at 7 DIV in *Slc12a6*^{+/+} motoneurons. In *Slc12a6*^{-/-} motoneurons, *in vitro* maturation still induced a 20 mV shift of $E_{\text{GABA-A}}$ from -62 ± 3 mV ($n = 10$) at 1 DIV to -82 ± 4 mV ($n = 8$) at 7 DIV (Fig.4G). The corresponding $[\text{Cl}^-]_i$, calculated with the Nernst equation, showed this concentration to be 17 ± 2 mM and 13 ± 2 mM at 1 DIV, decreasing to 7 ± 1 mM and 6 ± 1 mM, at 7 DIV, in *Slc12a6*^{+/+} and *Slc12a6*^{-/-} motoneurons, respectively ($P < 0.001$ between 1 and 7 DIV for both genotypes, *t*-test). Thus, loss of KCC3 does not alter the $[\text{Cl}^-]_i$ of 1 and 7 DIV motoneurons, suggesting that $[\text{Cl}^-]_i$ -dependent excitability is not affected in *Slc12a6*^{-/-} motoneurons.

Loss of KCC3 alters firing properties of motoneurons

Besides chloride regulation, KCC3 activity is known to induce changes in intracellular K^+ concentration, which in turn could modify the Na^+/K^+ ATPase (NKA) activity as well as other related ionic channels (Fujii et al., 2010; Adragna et al., 2015). Therefore, we compared the electrical properties of *Slc12a6*^{+/+} and *Slc12a6*^{-/-} motoneurons at 7-8 DIV, an *in vitro* time point at which we have previously shown motoneuron cultures reach electrical maturation (Camu et al., 2014). Due to the lack of neuromodulatory control, primary cultures allow the analysis of the primary range of motoneuron firing properties exclusively (Brownstone, 2006; Heckman et al., 2009). We found no significant differences in whole cell capacitance (54.3 ± 3.3 pF, $n = 13$ for *Slc12a6*^{+/+} motoneurons and 58.0 ± 3.7 pF, $n = 19$ for *Slc12a6*^{-/-} motoneurons, *t*-test) and in input resistance (218 ± 16 M Ω and 188 ± 17 M Ω for *Slc12a6*^{+/+} and *Slc12a6*^{-/-} motoneurons, respectively, *t*-test). We also saw no differences in resting membrane potential, action potential amplitude and duration (Fig. 5A-C). Further, motoneurons from both genotypes were able to fire repetitive action potentials under application of a 500 ms depolarizing current (Fig. 5D) and their frequency-current

relationships were similar (Fig. 5E). However, a salient feature of KCC3 deletion was the progressive depolarization of the amplitude of the after hyperpolarization (AHP) of each action potential during a train of activity, while it remained constant in *Slc12a6*^{+/+} motoneuron (Fig. 5D, F). Moreover, the appearance of hyperpolarization following a train of action potentials, known as post-tetanic hyperpolarization (PTH), was significantly reduced in *Slc12a6*^{-/-} motoneurons (Fig. 5D, G).

As the cation-chloride co-transporters are electroneutral, the depolarization of plateau potential observed in *Slc12a6*^{-/-} motoneurons cannot be due to the loss of KCC3 activity *per se* and is most likely the result of a disturbed electrogenic mechanism. The ionic currents governing plateau potential of motoneurons in primary culture and potentially linked to KCC3 activity are the K⁺ and Cl⁻ channels and the NKA (del Negro et al., 1999; Brownstone, 2006). Due to the lack of differences in action potentials duration, voltage-dependent K⁺ currents were excluded from the candidates. Analysis of the effects of Ca²⁺-activated K⁺ (BK and SK) currents using either CdCl₂, a non-specific inhibitor of voltage-gated Ca²⁺ currents (Fig. 6A, B) or apamin, a specific SK channel inhibitor (Fig. 6C, D), shows an increase in firing frequency without significant modification of plateau potential of wildtype motoneurons, thus ruling out their contribution to the depolarization observed in *Slc12a6*^{-/-} motoneuron. There is no report of voltage-gated Cl⁻ currents being expressed in motoneurons, and the effects of CdCl₂ rule out the contribution of a Ca²⁺ activated Cl⁻ current. We next analyzed the effects of ouabain, an inhibitor of NKA on motoneuron electrical activity. At 3 and 10 μM, ouabain had no effects on electrical activity. At 100 μM, it induced a 4 mV shift of the plateau potential towards more depolarized values during repetitive activity (Fig. 6E, F). Although the RMP was not significantly modified (-64 ± 2 mV in control condition and -59 ± 6 mV 2 minutes after ouabain application, *n* = 7), the PTH decreased from -1.16 ± 0.27 mV to -0.22 ± 0.25 mV, *n* = 7, *p* = 0.02 (Fig. 6G). We also observed that, under extracellular loose patch-clamp,

at least 100 μ M ouabain were necessary to increase motoneuron spontaneous firing frequency (not shown).

Altogether, our results suggest that loss of KCC3 promotes the reduction of an activity-dependent hyperpolarizing current that could be related to a progressive decrease in NKA pump current.

Motoneuron excitability contributes to NMJ denervation in $Slc12a6^{-/-}$ mice

Having established the potential neuronal origin of NMJ denervation and an activity-dependent reduction in hyperpolarizing current, we aimed to verify whether a causative relationship could exist between $Slc12a6^{-/-}$ motoneuron excitability and innervation of NMJs, as previously reported in early stages of various neuromuscular and neurodegenerative diseases (Kanai et al., 2006; Liu et al., 2015). To decrease motoneuron electrical activity *in vivo*, we used carbamazepine (CBZ), a clinically-approved molecule for the treatment of hyperexcitability-related disorders such as epilepsy or neuropathic pain (Bialer, 2012). We first deciphered the effects of CBZ on motoneurons by analyzing its effects on 7 DIV *Hb9::GFP* motoneurons isolated from the ventral horn spinal cord of E12.5 embryos without purification steps, which allows the recording of a synaptically-driven spontaneous activity (Fig. 7A, B). Acute application of 10 μ M CBZ did not modify spontaneous motoneuron activity while, at 100 μ M, CBZ decreased the frequency of spontaneous motoneuron activity without apparent reduction in spike amplitude.

Having established that CBZ decreases spontaneous motoneuron activity without effects on spike amplitude, its effect on NMJ innervation was evaluated by daily intraperitoneal injections to $Slc12a6^{-/-}$ mice from P10 to P30 (0.025 mg/g). By analyzing TA muscles from vehicle- and CBZ-treated $Slc12a6^{-/-}$ mice, we found that CBZ-treated $Slc12a6^{-/-}$

mice display significantly more fully innervated NMJs than vehicle-treated *Slc12a6*^{-/-} mice (Fig. 7C, D). In addition, nerve terminals of partially innervated CBZ-treated NMJs appeared to cover a greater area of the endplate than vehicle-treated NMJs (Fig. 7C, arrows).

These data, together with the role of NKA pump in maintenance of the plateau potential of motoneurons, led us to investigate further the expression of NKA in large α -motoneurons of the ventral region of the spinal cord. As previously reported (Edwards et al., 2013), the specific membrane expression of NKA α 1 subunit is a marker of large cholinergic motoneurons (Fig. 7E). Strikingly, NKA α 1 displays a non-uniform pattern around the cell body perimeter of *Slc12a6*^{-/-} motoneurons as opposed to the homogeneous pattern in wildtype motoneurons (Fig. 7E). To quantify this uneven localization of NKA α 1 around the cell perimeter of *Slc12a6*^{-/-} motoneurons, we measured the NKA α 1 staining intensity along the membrane and used the standard deviation (SD) as a read-out for heterogeneous expression. Indeed, a small SD is indicative of a uniform staining pattern while a high SD suggests uneven distribution along cell body perimeter. Our analysis shows that the average SD of NKA α 1 staining intensity along the membrane is significantly greater in *Slc12a6*^{-/-} motoneurons than in *Slc12a6*^{+/+} cells (Fig. 7F, left). Importantly, *in vivo* CBZ treatment restores NKA α 1 staining intensity along the membrane of *Slc12a6*^{-/-} motoneurons (Fig. 7E-F, right).

Modifications in NKA α 1 expression in motoneurons together with the effects of the activity-targeting drug CBZ on NMJ innervation provide strong support to a contribution of motoneuron activity to the neurodegenerative events that occur in *Slc12a6*^{-/-} animals.

Discussion

Our results reveal the role of electrical activity in the process of NMJ denervation and subsequent neurodegeneration in Andermann syndrome. We found that loss of KCC3 function is associated with an abnormal intrinsic neuronal electrical activity. Notably, we show that pharmacologically decreasing the firing frequency of *Slc12a6*^{-/-} motoneurons partially rescues innervation at the NMJ.

Our study shows for the first time that prior to axonal degeneration, significant pre- and post-synaptic NMJ defects accompany skeletal myofiber atrophy, which can account for the early locomotor abnormalities observed in young *Slc12a6*^{-/-} mice (Howard et al., 2002). This observation suggests that early denervation could as well contribute to axon swelling and myelin destruction, as described in nerve injury models (Vargas and Barres, 2007) and neurodegenerative diseases such as amyotrophic lateral sclerosis, in which the earliest pre-symptomatic functional and pathological changes observed occur distally in axons and at the NMJ (Moloney et al., 2014). The NMJ is a tri-partite synapse, composed of the skeletal muscle fiber, the motoneuron terminal and several terminal Schwann cells and any disturbance in these elements can induce denervation. The role of excitability in neurodegenerative diseases is unclear and, depending on the cellular pathological context, motoneuron hyperexcitability either promotes NMJ denervation (Rueggsegger et al., 2015) or protects against it (Saxena et al., 2013). Here, using the neuron-specific *Slc12a6*^{-/-} mice, we provide evidence that aberrant motoneuron activity is responsible for NMJ denervation at the TA muscle and that by decreasing motoneuron firing frequency via CBZ, we could slow down the denervation process in *Slc12a6*^{-/-} mice. Together, our data suggest that KCC3-dependent excitability is detrimental to NMJ maintenance, which is consistent with the absence of NMJ neurotransmission defects in ACCPN patients.

Several possibilities could account for the neuronal specific effects of KCC3. First, the expression of the short KCC3a isoform is enriched in spinal cord and motoneurons compared to skeletal muscle. Nothing is known about the function and molecular interactions of this isoform and it will be of great interest to further decipher its role in the nervous system. Second, the neuronal effects could be related to electrical activity. We show that in the spinal cord and motoneurons, the chloride shift and the increased expression of KCC2 still occur in the absence of KCC3, suggesting that the molecular mechanisms that regulate inhibitory neurotransmission correctly take place in *Slc12a6*^{-/-} mice. At 7 DIV, roughly 20 mV more depolarized values of RMP compared to $E_{\text{GABA-A}}$ confirm similar hyperpolarizing effects of GABAergic transmission in electrically mature motoneurons of both genotypes as reported in spinal cord developmental studies (Delpy et al., 2008; Stil et al., 2009). Quantitatively, there is a factor of 10 in the fold change in KCC2 transcripts expression in spinal cord compared to isolated motoneurons, which could be related to the presence of interneurons in spinal cord and suggests that regulation of KCC2 expression is more moderate in motoneurons than in interneurons or dorsal horn. KCC2 protein expression increases until the end of the first post-natal week both in ventral and dorsal horn (Stil et al., 2009) and the chloride switch in rat dorsal horn occurs at P0-P1 in 60 % of neurons and is completed by P7 (Baccei and Fitzgerald, 2004; Cordero-Erausquin et al., 2005). Despite discrepancies between transcript and protein levels between spinal cord and primary motoneuron culture, chloride extrusion capacity in isolated motoneurons is quite efficient and could also be related to other buffering system. While extrapolating data from embryonic cultured motoneurons to adult neurons *in vivo* comes with caveats, the resting $[\text{Cl}^-]_i$ in 7DIV cultured E12.5 motoneurons is not different from that found in mature cells (Delpy et al., 2008; Stil et al., 2009) and thus allows for some cautious inferences. The increase in NKCC1 transcript at a later stage in spinal cord is probably related to non-neuronal cells (Stil et al., 2009). Its overexpression in *Slc12a6*^{-/-}

spinal cords needs further investigation at protein and cellular levels. Altogether, our results rule out a direct role for KCC3 in the control of chloride-driven motoneuron electrical activity.

Analysis of firing properties of purified motoneurons at 8 DIV shows that frequency-current relationship reaches a plateau level around 20-30 Hz within 150 pA without changes in slope following a higher current amplitude. Most studies in spinal motoneurons, performed on P8-P15 slices, describe two levels of firing: a primary range at a maximal 40 Hz attributed to intrinsic motoneuron properties followed by a secondary range attributed to ionotropic and neuromodulatory influences (Brownstone, 2006; Heckman et al., 2009). Contrary to *in vivo* recordings, the absence of synaptic inputs and descending pathways in the highly purified motoneuron cultures prevents recordings of the secondary range of firing. Comparison of motoneuron electrical properties with *in situ* slice recordings shows that the major difference with post-natal motoneurons concerns values of input resistance, which are higher in primary cultures, accounting for their lower threshold current amplitude (Carrascal et al., 2005). More recently, recordings from adult mouse slices show that input resistance is closer to primary cultures than post-natal slices, which account for similar relationship between current amplitude and corresponding frequency (Mitra and Brownstone, 2012). In addition to the f-I relation, we show that apamin is able to increase firing frequency, as reported in post-natal P9-P15 spinal cord slices recordings (Miles et al., 2007), supporting functional modulatory mechanisms in primary cultures. Using purified motoneurons, we demonstrate that KCC3 deletion does not modify the f-I relation, but induces a progressive depolarization of plateau potential during rhythmic activity. Among the candidates tested, Ca^{2+} activated K^{+} currents and the NKA, only inhibition of NKA was able to induce a depolarization of the plateau potential suggesting that ionic unbalance progressively takes place during maintained activity in the absence of KCC3. In addition, we show in spinal cord that plasma membrane

expression of the $\alpha 1$ -subunit of NKA is modified in the absence of functional KCC3. Interestingly, the expression of NKA α subunits in spinal cord is not pan-motoneuronal as two recent studies show that the $\alpha 1$ subunit is a marker of a subpopulation of large α -motoneurons including the fast resistant (FR) and the slow (S) motoneurons, while the $\alpha 3$ subunit is mainly a marker of the fast fatigable (FF) α -motoneurons and the small γ -motoneurons innervating intrafusal muscle fibers (Edwards et al., 2013; Ruegsegger et al., 2015). The NKA is an electrogenic ion pump essential for maintenance of cellular electrochemical gradients (Kaplan, 2002) and activity-dependent changes in NKA pump can alter the hyperpolarizing pump current (Scuri et al., 2002; Kim et al., 2007). Although we cannot state whether activity of the pump is directly affected by KCC3 loss of function, our results are in line with studies showing that KCC3 hyperactivity increases NKA activity (Adragna et al., 2015) while KCC3 inhibition has the inverse effect (Fujii et al., 2008). Moreover, decreased NKA activity induces NMJ denervation (Ruegsegger et al., 2015). Remarkably, by decreasing motoneuron firing frequency, CBZ restore Na^+K^+ -ATPase $\alpha 1$ localization. While membrane pattern of the pump is fully restored, CBZ treatment cannot promote full NMJ reinnervation suggesting that its effects slow denervation process and/or that denervation is not reversible. These data also suggest that the membrane redistribution of the NKA $\alpha 1$ -subunit might be a consequence of the hyperexcitable state induced by the decreased activity of the pump in *Slc12a6*^{-/-} motoneurons, an observation that needs further investigation on the cellular mechanisms linking protein activity and localization. Additional mechanisms may also contribute to the impaired locomotor capacities described in *Slc12a6*^{-/-} mice. Indeed, it has recently been demonstrated that the selective deletion of *Slc12a6* in parvalbumin-positive proprioceptive neurons is sufficient to induce locomotor defects (Ding and Delpire, 2014), which could be linked to an increased pre-synaptic inhibition of a subset of sensory neurons (Lucas et al., 2012).

Conclusion

Overall, our results highlight novel pathological hallmarks and molecular effectors within the motor circuitry of Andermann syndrome. Of utmost importance is the targeting of motoneuron excitability with CBZ to maintain some innervation in *Slc12a6*^{-/-} mice. These findings have major clinical implications as they bring forward novel symptomatic and molecular therapeutic targets for the treatment and clinical management of ACCPN patients.

Acknowledgements

We are grateful to Dr Jacques Deléan for his help with the EMG drawings, Dr Lyndsay M. Murray and Dr Inna Uliyakina for helpful discussions, the personnel of the réseau d'histologie expérimentale de Montpellier, the Montpellier RIO Imaging and the INM animal facility for their services.

Funding sources

M.B. was a recipient of an EMBO long-term fellowship and is currently an SMA Trust Career Development Fellow. E.D. is supported by NIH grant GM74771. E.C was a recipient of an association française contre les myopathies (AFM) Ph.D fellowship. This work was supported by grants from the institut national de la santé et de la recherche médicale (Inserm), the association française pour la recherche sur la SLA (ARSLA), ANR-14-RARE-0006 E-RARE FaSMALS, ANR GliALS and AFM.

Conflicts of Interest

The authors declare that they have no conflicts of interest

References

- Adragna NC, Ravilla NB, Lauf PK, Begum G, Khanna AR, Sun D, Kahle KT (2015) Regulated phosphorylation of the K-Cl cotransporter KCC3 is a molecular switch of intracellular potassium content and cell volume homeostasis. *Front Cell Neurosci* 9, 255.
- Allain AE, Le Corrionc H, Delpy A, Cazenave W, Meyrand P, Legendre P, Branchereau P (2011) Maturation of the GABAergic transmission in normal and pathologic motoneurons. *Neural Plast* 2011, 905624. doi: 905610.901155/902011/905624.
- Arce V, Garces A, de Bovis B, Filippi P, Henderson C, Pettmann B, deLapeyriere O (1999) Cardiotrophin-1 requires LIFRbeta to promote survival of mouse motoneurons purified by a novel technique. *J Neurosci Res* 55, 119-126.
- Baccai ML, Fitzgerald M (2004) Development of GABAergic and glycinergic transmission in the neonatal rat dorsal horn. *J Neurosci* 24, 4749-4757.
- Berrih-Aknin S, Frenkian-Cuvelier M, Eymard B (2014) Diagnostic and clinical classification of autoimmune myasthenia gravis. *J Autoimmun* 48-49, 143-148. doi: 110.1016/j.jaut.2014.1001.1003.
- Bialer M (2012) Why are antiepileptic drugs used for nonepileptic conditions? *Epilepsia* 53 Suppl 7, 26-33.
- Blaesse P, Airaksinen MS, Rivera C, Kaila K (2009) Cation-chloride cotransporters and neuronal function. *Neuron* 61, 820-838.
- Boettger T, Rust MB, Maier H, Seidenbecher T, Schweizer M, Keating DJ, Faulhaber J, Ehmke H, Pfeiffer C, Scheel O, Lemcke B, Horst J, Leuwer R, Pape HC, Volkl H, Hubner CA, Jentsch TJ (2003) Loss of K-Cl co-transporter KCC3 causes deafness, neurodegeneration and reduced seizure threshold. *Embo J* 22, 5422-5434.
- Bowerman M, Murray LM, Beauvais A, Pinheiro B, Kothary R (2012) A critical smn threshold in mice dictates onset of an intermediate spinal muscular atrophy phenotype associated with a distinct neuromuscular junction pathology. *Neuromuscul Disord* 22, 263-276.
- Brownstone RM (2006) Beginning at the end: repetitive firing properties in the final common pathway. *Prog Neurobiol* 78, 156-172.
- Byun N, Delpire E (2007) Axonal and periaxonal swelling precede peripheral neurodegeneration in KCC3 knockout mice. *Neurobiol Dis* 28, 39-51.
- Camu W, Tremblier B, Plassot C, Alphonso S, Salsac C, Pageot N, Juntas-Morales R, Scamps F, Daures JP, Raoul C (2014) Vitamin D confers protection to motoneurons and is a prognostic factor of amyotrophic lateral sclerosis. *Neurobiol Aging* 35, 1198-1205.
- Carrascal L, Nieto-Gonzalez JL, Cameron WE, Torres B, Nunez-Abades PA (2005) Changes during the postnatal development in physiological and anatomical characteristics of rat motoneurons studied in vitro. *Brain Res Brain Res Rev* 49, 377-387.
- Cordero-Erausquin M, Coull JA, Boudreau D, Rolland M, De Koninck Y (2005) Differential maturation of GABA action and anion reversal potential in spinal lamina I neurons: impact of chloride extrusion capacity. *J Neurosci* 25, 9613-9623.
- DeBraekeleer M, Dallaire A, Mathieu J (1993) Genetic epidemiology of sensorimotor polyneuropathy with or without agenesis of the corpus callosum in northeastern Quebec. *Hum Genet* 91, 223-227.

- del Negro CA, Hsiao CF, Chandler SH (1999) Outward currents influencing bursting dynamics in guinea pig trigeminal motoneurons. *J Neurophysiol* 81, 1478-1485.
- Delpy A, Allain AE, Meyrand P, Branchereau P (2008) NKCC1 cotransporter inactivation underlies embryonic development of chloride-mediated inhibition in mouse spinal motoneuron. *J Physiol* 586, 1059-1075.
- Ding J, Delpire E (2014) Deletion of KCC3 in parvalbumin neurons leads to locomotor deficit in a conditional mouse model of peripheral neuropathy associated with agenesis of the corpus callosum. *Behav Brain Res* 274, 128-136.
- Dupre N, Howard HC, Mathieu J, Karpati G, Vanasse M, Bouchard JP, Carpenter S, Rouleau GA (2003) Hereditary motor and sensory neuropathy with agenesis of the corpus callosum. *Ann Neurol* 54, 9-18.
- Edwards IJ, Bruce G, Lawrenson C, Howe L, Clapcote SJ, Deuchars SA, Deuchars J (2013) Na⁺/K⁺ ATPase alpha1 and alpha3 isoforms are differentially expressed in alpha- and gamma-motoneurons. *J Neurosci* 33, 9913-9919.
- Fujii T, Fujita K, Shimizu T, Takeguchi N, Sakai H (2010) The NH(2)-terminus of K(+)Cl(-) cotransporter 3a is essential for up-regulation of Na(+),K(+)-ATPase activity. *Biochem Biophys Res Commun* 399, 683-687.
- Fujii T, Takahashi Y, Itomi Y, Fujita K, Morii M, Tabuchi Y, Asano S, Tsukada K, Takeguchi N, Sakai H (2008) K⁺-Cl⁻ Cotransporter-3a Up-regulates Na⁺,K⁺-ATPase in Lipid Rafts of Gastric Luminal Parietal Cells. *J Biol Chem* 283, 6869-6877.
- Gagnon KB, Delpire E (2013) Physiology of SLC12 transporters: lessons from inherited human genetic mutations and genetically engineered mouse knockouts. *Am J Physiol Cell Physiol* 304, C693-714.
- Heckman CJ, Mottram C, Quinlan K, Theiss R, Schuster J (2009) Motoneuron excitability: the importance of neuromodulatory inputs. *Clin Neurophysiol* 120, 2040-2054.
- Hiki K, D'Andrea RJ, Furze J, Crawford J, Woollatt E, Sutherland GR, Vadas MA, Gamble JR (1999) Cloning, characterization, and chromosomal location of a novel human K⁺-Cl⁻ cotransporter. *J Biol Chem* 274, 10661-10667.
- Howard HC, Mount DB, Rochefort D, Byun N, Dupre N, Lu J, Fan X, Song L, Riviere JB, Prevost C, Horst J, Simonati A, Lemcke B, Welch R, England R, Zhan FQ, Mercado A, Siesser WB, George AL, Jr., McDonald MP, Bouchard JP, Mathieu J, Delpire E, Rouleau GA (2002) The K-Cl cotransporter KCC3 is mutant in a severe peripheral neuropathy associated with agenesis of the corpus callosum. *Nat Genet* 32, 384-392.
- Hubner CA, Stein V, Hermans-Borgmeyer I, Meyer T, Ballanyi K, Jentsch TJ (2001) Disruption of KCC2 reveals an essential role of K-Cl cotransport already in early synaptic inhibition. *Neuron* 30, 515-524.
- Kanai K, Kuwabara S, Misawa S, Tamura N, Ogawara K, Nakata M, Sawai S, Hattori T, Bostock H (2006) Altered axonal excitability properties in amyotrophic lateral sclerosis: impaired potassium channel function related to disease stage. *Brain* 129, 953-962.
- Kaplan JH (2002) Biochemistry of Na,K-ATPase. *Annu Rev Biochem* 71, 511-535.
- Kim JH, Sizov I, Dobretsov M, von Gersdorff H (2007) Presynaptic Ca²⁺ buffers control the strength of a fast post-tetanic hyperpolarization mediated by the alpha3 Na(+)/K(+)-ATPase. *Nat Neurosci* 10, 196-205.
- Larbrisseau A, Vanasse M, Brochu P, Jasmin G (1984) The Andermann syndrome: agenesis of the corpus callosum associated with mental retardation and progressive sensorimotor neuronopathy. *Can J Neurol Sci* 11, 257-261.
- Le Rouzic P, Ivanov TR, Stanley PJ, Baudoin FM, Chan F, Pinteaux E, Brown PD, Luckman SM (2006) KCC3 and KCC4 expression in rat adult forebrain. *Brain Res* 1110, 39-45.

- Li B, Hertz L, Peng L (2013) Cell-specific mRNA alterations in Na⁺, K⁺-ATPase alpha and beta isoforms and FXYD in mice treated chronically with carbamazepine, an anti-bipolar drug. *Neurochem Res* 38, 834-841.
- Liu H, Lu J, Chen H, Du Z, Li XJ, Zhang SC (2015) Spinal muscular atrophy patient-derived motor neurons exhibit hyperexcitability. *Sci Rep* 5, 12189.
- Lucas O, Hilaire C, Delpire E, Scamps F (2012) KCC3-dependent chloride extrusion in adult sensory neurons. *Mol Cell Neurosci* 50, 211-220.
- Mathieu J, Bedard F, Prevost C, Langevin P (1990) [Motor and sensory neuropathies with or without agenesis of the corpus callosum: a radiological study of 64 cases.]. *Can J Neurol Sci* 17, 103-108.
- Mercado A, Vazquez N, Song L, Cortes R, Enck AH, Welch R, Delpire E, Gamba G, Mount DB (2005) NH₂-terminal heterogeneity in the KCC3 K⁺-Cl⁻ cotransporter. *Am J Physiol Renal Physiol* 289, F1246-1261.
- Miles GB, Hartley R, Todd AJ, Brownstone RM (2007) Spinal cholinergic interneurons regulate the excitability of motoneurons during locomotion. *Proc Natl Acad Sci U S A* 104, 2448-2453.
- Mitra P, Brownstone RM (2012) An in vitro spinal cord slice preparation for recording from lumbar motoneurons of the adult mouse. *J Neurophysiol* 107, 728-741.
- Moloney EB, de Winter F, Verhaagen J (2014) ALS as a distal axonopathy: molecular mechanisms affecting neuromuscular junction stability in the presymptomatic stages of the disease. *Front Neurosci* 8, 252.
- Mount DB, Mercado A, Song L, Xu J, George AL, Jr., Delpire E, Gamba G (1999) Cloning and characterization of KCC3 and KCC4, new members of the cation-chloride cotransporter gene family. *J Biol Chem* 274, 16355-16362.
- O'Neill WC (1999) Physiological significance of volume-regulatory transporters. *Am J Physiol* 276, C995-C1011.
- Pieraut S, Laurent-Matha V, Sar C, Hubert T, Mechaly I, Hilaire C, Mersel M, Delpire E, Valmier J, Scamps F (2007) NKCC1 phosphorylation stimulates neurite growth of injured adult sensory neurons. *J Neurosci* 27, 6751-6759.
- Race JE, Makhoul FN, Logue PJ, Wilson FH, Dunham PB, Holtzman EJ (1999) Molecular cloning and functional characterization of KCC3, a new K-Cl cotransporter. *Am J Physiol* 277, C1210-1219.
- Raoul C, Henderson CE, Pettmann B (1999) Programmed cell death of embryonic motoneurons triggered through the Fas death receptor. *J Cell Biol* 147, 1049-1062.
- Raoul C, Estevez AG, Nishimune H, Cleveland DW, deLapeyriere O, Henderson CE, Haase G, Pettmann B (2002) Motoneuron death triggered by a specific pathway downstream of Fas. potentiation by ALS-linked SOD1 mutations. *Neuron* 35, 1067-1083.
- Rivera C, Voipio J, Payne JA, Ruusuvuori E, Lahtinen H, Lamsa K, Pirvola U, Saarma M, Kaila K (1999) The K⁺/Cl⁻ co-transporter KCC2 renders GABA hyperpolarizing during neuronal maturation. *Nature* 397, 251-255.
- Rueggsegger C, Maharjan N, Goswami A, de L'Etang AF, Weis J, Troost D, Heller M, Gut H, Saxena S (2015) Aberrant association of misfolded SOD1 with Na/KATPase-alpha3 impairs its activity and contributes to motor neuron vulnerability in ALS. *Acta Neuropathol*.
- Saxena S, Roselli F, Singh K, Leptien K, Julien JP, Gros-Louis F, Caroni P (2013) Neuroprotection through excitability and mTOR required in ALS motoneurons to delay disease and extend survival. *Neuron* 80, 80-96.
- Scuri R, Mozzachiodi R, Brunelli M (2002) Activity-dependent increase of the AHP amplitude in T sensory neurons of the leech. *J Neurophysiol* 88, 2490-2500.

- Shekarabi M, Moldrich RX, Rasheed S, Salin-Cantegrel A, Laganriere J, Rochefort D, Hince P, Huot K, Gaudet R, Kurniawan N, Sotocinal SG, Ritchie J, Dion PA, Mogil JS, Richards LJ, Rouleau GA (2012) Loss of neuronal potassium/chloride cotransporter 3 (KCC3) is responsible for the degenerative phenotype in a conditional mouse model of hereditary motor and sensory neuropathy associated with agenesis of the corpus callosum. *J Neurosci* 32, 3865-3876.
- Stil A, Liabeuf S, Jean-Xavier C, Brocard C, Viemari JC, Vinay L (2009) Developmental up-regulation of the potassium-chloride cotransporter type 2 in the rat lumbar spinal cord. *Neuroscience* 164, 809-821.
- Sun YT, Lin TS, Tzeng SF, Delpire E, Shen MR (2010) Deficiency of electroneutral K⁺-Cl⁻ cotransporter 3 causes a disruption in impulse propagation along peripheral nerves. *Glia* 58, 1544-1552.
- Vargas ME, Barres BA (2007) Why is Wallerian degeneration in the CNS so slow? *Annu Rev Neurosci* 30, 153-179.
- Yan Y, Dempsey RJ, Sun D (2001) Expression of Na⁽⁺⁾-K⁽⁺⁾-Cl⁽⁻⁾ cotransporter in rat brain during development and its localization in mature astrocytes. *Brain Res* 911, 43-55.

Figure legends

Figure 1. Neuromuscular junction denervation is an early marker of *Slc12a6*^{-/-} associated neuropathy. (A) Representative images of lumbar spinal cord cross-sections from *Slc12a6*^{+/+} and *Slc12a6*^{-/-} stained with SMI32 antibody to morphologically identify the large motoneurons within the ventral horn region. Scale bar = 100 μ m. (B) Counts of SMI32-labelled large motoneuron cell bodies per section of ventral lumbar spinal cords show no difference between *Slc12a6*^{+/+} (7.28 ± 0.81 motoneurons/section, $n = 34$ sections; $N = 3$ mice) and *Slc12a6*^{-/-} (7.00 ± 0.64 motoneurons/section, $n = 54$ sections; $N = 4$ mice; non-significant, ns; Student's *t*-test). Scale bar, 100 μ m. (C) Images of complete and partially innervated NMJ immunolabeled with neurofilament (NF; green) and synaptic vesicle (SV2; green) antibodies to visualize the nerve terminal and with alpha-bungarotoxin (α BTX; red) to identify the NMJ endplate. (D) Analysis of NMJs in whole tibialis anterior (TA) muscles shows a 25 % increase in incomplete innervation in P30 *Slc12a6*^{-/-} mice (0.76 ± 0.76 %, $n = 112$ and 18.96 ± 5.24 %, $n = 157$ endplates from *Slc12a6*^{+/+} and *Slc12a6*^{-/-}, respectively; $N = 4$ TA muscles from 4 mice for each condition; $*P < 0.05$, Student's *t*-test). Scale bar: 5 μ m. (E-G) Electron micrographs of NMJs from the TA muscle of *Slc12a6*^{+/+} and *Slc12a6*^{-/-} mice (E). Upper left panel shows a typical NMJ in *Slc12a6*^{+/+} where the nerve terminal (T) faces a muscle cell (MC) and is capped by terminal Schwann cell (TSC) processes (arrows). In *Slc12a6*^{-/-} muscle, smaller NMJs are observed (upper right panel) and display shrunk terminals capped with TSC processes (lower left panel) or are even devoid of a nerve terminal (asterisk in lower right panel). (F) NMJs of *Slc12a6*^{-/-} mice (1.17 ± 0.17 μ m², $n = 38$) are smaller than *Slc12a6*^{+/+} mice (2.52 ± 0.31 μ m², $n = 43$; $***P < 0.001$; Student's *t*-test). Scale bars: 500 nm. (G) Evaluation of the innervation status of NMJs shows a greater proportion of *Slc12a6*^{-/-} NMJs with partial innervation of the terminal area (42.05 ± 17.05 %, $n = 38$) compared to *Slc12a6*^{+/+} NMJs (100 % innervation, $n = 43$; $***P < 0.001$; Fisher's exact test). $N = 2$ mice

for each condition; $n = 38$ terminals for *Slc12a6*^{-/-} mice and $n = 43$ terminals for *Slc12a6*^{+/+} mice.

Figure 2. Pre-synaptic defects contribute to post-synaptic neuromuscular junction disorganization and skeletal muscle atrophy in KCC3-deleted mice. (A-C) Morphological analysis of mature pretzel-like and disorganized (perforations with bright lines or plaque-like) NMJ endplates from TA muscles identified with α -Bungarotoxin-555 (A) shows more disorganized endplates in *Slc12a6*^{-/-} mice (B) and in neuron-specific *nsSlc12a6* ^{$\Delta 18/\Delta 18$} mice (C) than in *Slc12a6*^{+/+} mice. (7.42 ± 2.39 %, $n = 167$ and 37.88 ± 3.53 %, $n = 157$ endplates for *Slc12a6*^{+/+} and *Slc12a6*^{-/-}, respectively; $N = 5$ TA in (B) and 22.986 ± 2.85 %, $n = 78$ and 42.31 ± 6.41 %, $n = 84$ endplates for *Slc12a6*^{+/+} and *Slc12a6* ^{$\Delta 18/\Delta 18$} , respectively; $N = 3$ for each condition in (C); $**P < 0.01$; Fisher's exact test); scale bar: 5 μ m. (D,E) Myofibers of *Slc12a6*^{-/-} mice have smaller area (383 ± 21 μ m², $n = 3125$ myofibers) than their littermate *Slc12a6*^{+/+} mice (553 ± 48 μ m², $n = 2190$ myofibers) and (F,G) neuron-specific *nsSlc12a6* ^{$\Delta 18/\Delta 18$} mice have smaller area compared to their littermate *Slc12a6*^{+/+} mice (540 ± 69 μ m², $n = 1008$ myofibers for *nsSlc12a6*^{+/+} and 247 ± 22 μ m², $n = 2507$ myofibers for *nsSlc12a6* ^{$\Delta 18/\Delta 18$}); $N = 3$ TA for each group; $*P < 0.05$ Student's *t*-test). Scale bars: 50 μ m. Cross-sections of hematoxylin and eosin coloration of paraffin-embedded TA muscles.

Figure 3. Neuromuscular transmission is unaffected in ACCPN patient. (A-C) There is no evidence of a decrement in amplitude of muscle compound action potential (CAP) with time in a control patient (A). A gravis myasthenia patient served as a positive control for neuromuscular transmission defects and is characterized by a significant ($> 10\%$) decrease in the CAP amplitude due to the decrease of post-synaptic acetylcholine receptors (B).

Amplitude of motor CAP is severely decreased in ACCPN patients (basal motor potential is 1.0 ± 0.1 mV, $n = 2$ compared with 9.1 ± 1.1 mV in 3 healthy patients; 35, 41 and 61 years old) and shows no significant decrease with repetitive stimulation (at 3 Hz motor potential amplitude remains constant 1.0 ± 0.1 mV in ACCPN patients and 9.1 ± 1.1 mV in the healthy patients) (C). Table shows the clinical evaluation of the two ACCPN patients.

Figure 4. Deletion of *Slc12a6* does not affect the developmental chloride shift. (A) Quantitative PCR of KCC3 transcript expression in the spinal cord at embryonic day 12.5 (E12.5), postnatal day 1 (P1), P15 and young adult (P30) ($n = 3$ for each group) shows a significant upregulation of KCC3 transcript during spinal cord development (one-way ANOVA; $*P < 0.05$). (B) Representative RT-PCRs showing the presence of KCC3 transcript isoforms in P30 adult spinal cord (SC), P15 and P30 tibialis anterior muscle and cultured motoneurons at 7 days *in vitro* (DIV). Spinal cord and motoneurons show preferential expression of the exon 2-deleted KCC3a transcript isoform while both KCC3a transcript isoforms (FL KCC3a = full length KCC3a; $\Delta 2$ -KCC3a = exon-2-deleted) are similarly expressed within muscle. KCC3b transcript is not expressed in motoneurons. (C) Quantitative PCR of KCC2 and (D) NKCC1 transcripts was performed on the lumbar spinal cord of E12.5, P1 and P30 *Slc12a6*^{+/+} and *Slc12a6*^{-/-} mice and expressed relative to E12.5. For KCC2 at P1: 15.9 ± 2.0 fold increase and 16.5 ± 2.3 fold increase from *Slc12a6*^{+/+} and *Slc12a6*^{-/-}, respectively; at P30: 22.2 ± 1.6 fold increase and 26.5 ± 6.4 fold increase from *Slc12a6*^{+/+} and *Slc12a6*^{-/-}, respectively. $n = 3$ cultures for each group. For NKCC1 at P1: 1.65 ± 1.75 fold decrease and 0.36 ± 1.08 fold decrease from *Slc12a6*^{+/+} and *Slc12a6*^{-/-}, respectively; at P30: 7.5 ± 1.1 fold increase and 15.4 ± 3.6 fold increase from *Slc12a6*^{+/+} and *Slc12a6*^{-/-}, respectively. $n = 3$ cultures for each group. While loss of *Slc12a6* does not influence the

expression of KCC2 transcript, we find a significant upregulation of NKCC1 transcript during the developmental of *Slc12a6*^{-/-} spinal cord. The mRNA levels of each cation-chloride cotransporter were normalized to the relative expression of *Polr2j*, a housekeeping control gene. mRNA fold increase at different time points was obtained by dividing their expression by the values obtained at E12.5, which were not significantly different between groups (two-way ANOVA; **P* < 0.05). (E) Quantitative PCR was performed on enriched spinal motoneuron cultures isolated from E12.5 *Slc12a6*^{+/+} and *Slc12a6*^{-/-} spinal cord at 1 DIV and 7 DIV (for NKCC1: 1.45 ± 0.06 fold decrease, *n* = 4 and 1.73 ± 0.40, *n* = 3 from *Slc12a6*^{+/+} and *Slc12a6*^{-/-}, respectively. For KCC2: 2.6 ± 0.2 fold increase, *n* = 6 and 1.6 ± 0.4, *n* = 3 from *Slc12a6*^{+/+} and *Slc12a6*^{-/-}, respectively). Loss of KCC3 does not affect NKCC1 transcript levels while there is a significant 40 % decrease of KCC2 transcript during *in vitro* maturation of primary motoneurons. mRNA expression levels were first normalized to the relative expression level of *Polr2j*. mRNA changes for KCC2 and NKCC1 at 1 DIV were not different between each group (for KCC2: normalized expression was 1.3 ± 0.1 and 1.2 ± 0.3 for *Slc12a6*^{+/+} and *Slc12a6*^{-/-}, respectively and for NKCC1: normalized expression was 1.2 ± 0.1 and 1.1 ± 0.2 for *Slc12a6*^{+/+} and *Slc12a6*^{-/-}, respectively). Variation in gene expression during *in vitro* maturation was obtained by plotting the 7 DIV mRNA/1 DIV mRNA for each gene (two-way ANOVA). (F) Gramicidin-perforated patch clamp recordings showing currents evoked by the brief application of 50 μM muscimol on a wild type motoneuron at 7 DIV. Ramp protocols from -80 mV to +40 mV were applied every 5 seconds for measurement of the reversal potential, E_{GABA-A}, of the chloride current. (G) *Slc12a6* deletion does not modify the E_{GABA-A} of 1 DIV motoneurons and does not prevent the hyperpolarizing shift in E_{GABA-A} observed in 7 DIV motoneurons. The number of motoneurons analyzed is indicated in parentheses above their respective column (two-way ANOVA; ***P* < 0.01; ****P* < 0.001).

Figure 5. KCC3 contributes to plateau potential during sustained firing of motoneuron. (A) Representative traces of action potential (AP) recordings in 7 DIV *Slc12a6*^{+/+} (left) and *Slc12a6*^{-/-} motoneurons (right). (B) Resting membrane potential RMP (-59.6 ± 2.0 mV and -58.8 ± 1.5 mV in *Slc12a6*^{+/+} and *Slc12a6*^{-/-} motoneurons, respectively), the peak amplitude of the AP (48.1 ± 2.9 mV and 43.9 ± 1.7 mV in *Slc12a6*^{+/+} and *Slc12a6*^{-/-} motoneurons, respectively) and (C) the duration of the AP (1.10 ± 0.08 ms and 0.94 ± 0.04 ms in *Slc12a6*^{+/+} and *Slc12a6*^{-/-} motoneurons, respectively) are not significantly different between the two genotypes. The number of motoneurons is indicated in brackets. (two-way ANOVA; ns, not significant). (D) Representative current-clamp recordings of repetitive firing in *Slc12a6*^{+/+} and *Slc12a6*^{-/-} motoneurons elicited by supra-threshold (110 pA) current injection (500 ms duration). (E) Spike frequency *versus* injected current shows no significant differences between the two genotypes (multiple *t*-tests); the mean action potentials number at 110 pA was 10.1 ± 0.8 (range from 3-14) and 10.4 ± 0.7 (range 2-16) in *Slc12a6*^{+/+} and *Slc12a6*^{-/-} motoneurons, respectively. (F) Amplitude of the peak after hyperpolarization of each action potential during a repetitive activity (plateau AHP) induced with a 110 pA current injection plotted versus each of action potential (*i.e.* with time). This relationships shows that the plateau potential remains constant in *Slc12a6*^{+/+} motoneurons while it significantly depolarizes in *Slc12a6*^{-/-} motoneurons (multiple *t*-test; $*P < 0.05$, $**P < 0.01$). (G) Peak amplitude of the post-tetanic hyperpolarization, PTH in (D) was measured at the end of the 500 ms action potential train, following a supra-threshold current injection (110 pA). PTH is significantly decreased in *Slc12a6*^{-/-} motoneurons (-5.2 ± 0.6 mV, $n = 13$ and -2.8 ± 0.6 , $n = 19$ from *Slc12a6*^{+/+} and *Slc12a6*^{-/-} motoneurons, respectively; *t*-test; $*P < 0.05$).

Figure 6. Pharmacological characterization of ionic currents involved in plateau potential maintenance in 7 DIV *Slc12a6*^{+/+} motoneurons. (A) Inhibition of voltage-gated Ca^{2+} currents

with 100 μM CdCl_2 induces an increase in motoneuron firing frequency from 14.0 ± 3.2 Hz to 20.5 ± 2.9 Hz without significant change in plateau potential (**B**) ($n = 4$ motoneurons, $p < 0.05$, paired experiments). (**C,D**) Specific inhibition of the Ca^{2+} -activated K^+ current, SK channels, with apamin increases firing frequency from 11.7 ± 1.3 Hz to 17.3 ± 1.4 Hz by reducing the slope of the slow depolarization following a spike without changing the value of plateau potential ($n = 7$ motoneurons, $p < 0.001$, paired experiments). (**E**) Inhibition of the Na^+ - K^+ ATPase with 100 μM ouabain induces a significant depolarization of the plateau potential ($n = 7$, paired test, $** p < 0.01$), without changes in firing frequency (21.7 ± 1.9 Hz and 22.6 ± 1.8 Hz before and after ouabain, respectively; $n = 7$, $P = 0.7$) (**F**). (**G**) The amplitude of PTH is decreased from -1.16 ± 0.27 mV to -0.22 ± 0.25 mV following ouabain treatment ($n = 7$, paired test, $* p < 0.05$).

Figure 7. Motoneuron excitability contributes to *Slc12a6*^{-/-} neuromuscular junction innervation. (**A**) On line recordings of *in vitro* spontaneous electrical activity of *Hb9::GFP* motoneurons before and after cumulative application of 10 μM and 100 μM CBZ. (**B**) At 100 μM , CBZ induces a 60% decrease in firing frequency ($n = 3$; $**P < 0.01$; one way ANOVA). (**C**) Images of P30 NMJs from vehicle- and CBZ-treated *Slc12a6*^{-/-} mice showing full and partial innervation of whole TA muscles. Arrowheads indicate incomplete NMJ innervation. Scale bar: 50 μm . (**D**) Quantification of innervation status confirms that CBZ treatment increases the number of innervated NMJs in *Slc12a6*^{-/-} mice (60.9 ± 3.2 % of innervation) compared to vehicle-treated *Slc12a6*^{-/-}, (49.2 ± 1.7 % of innervation) but does not totally rescue the control phenotype (99 ± 1 % of innervation) (260, 710 and 260 endplates for *Slc12a6*^{+/+}, vehicle-treated *Slc12a6*^{-/-} and CBZ-treated *Slc12a6*^{-/-} respectively; $N = 3$ mice for each group, $**P < 0.01$; $***P < 0.001$; one-way ANOVA). (**E**) Spinal cord cross-sections of P30 *Slc12a6*^{+/+}, vehicle and CBZ-treated *Slc12a6*^{-/-} mice were immunolabeled with the

Na⁺/K⁺-ATPase (NKA) α 1 antibody and the motoneuron marker choline acetyl transferase (ChAT). Scale bar, 25 μ m. (F) Quantification of the standard deviation (SD) of NKA α 1 staining intensity along motoneuron membrane perimeter shows a significantly greater uneven distribution of NKA α 1 in *Slc12a6*^{-/-} spinal cord motoneurons (11.35 ± 0.36 SD, $n = 140$) compared to *Slc12a6*^{+/+} motoneurons (8.56 ± 0.24 SD, $n = 156$) ($N = 3$ mice for each group, *** $P < 0.001$; t-test; left panel). *In vivo* treatment with CBZ restores NKA α 1 staining intensity of motoneurons to control levels (8.47 ± 0.39 SD, $n = 124$, in *Slc12a6*^{+/+} motoneurons; 12.34 ± 0.49 SD, $n = 71$, in vehicle-treated *Slc12a6*^{-/-} mice, compared to 8.03 ± 0.30 SD, $n = 137$, in CBZ-treated *Slc12a6*^{-/-} mice; one-way ANOVA; right panel. $N = 3$ mice for each group).

Figure 1
[Click here to download high resolution image](#)

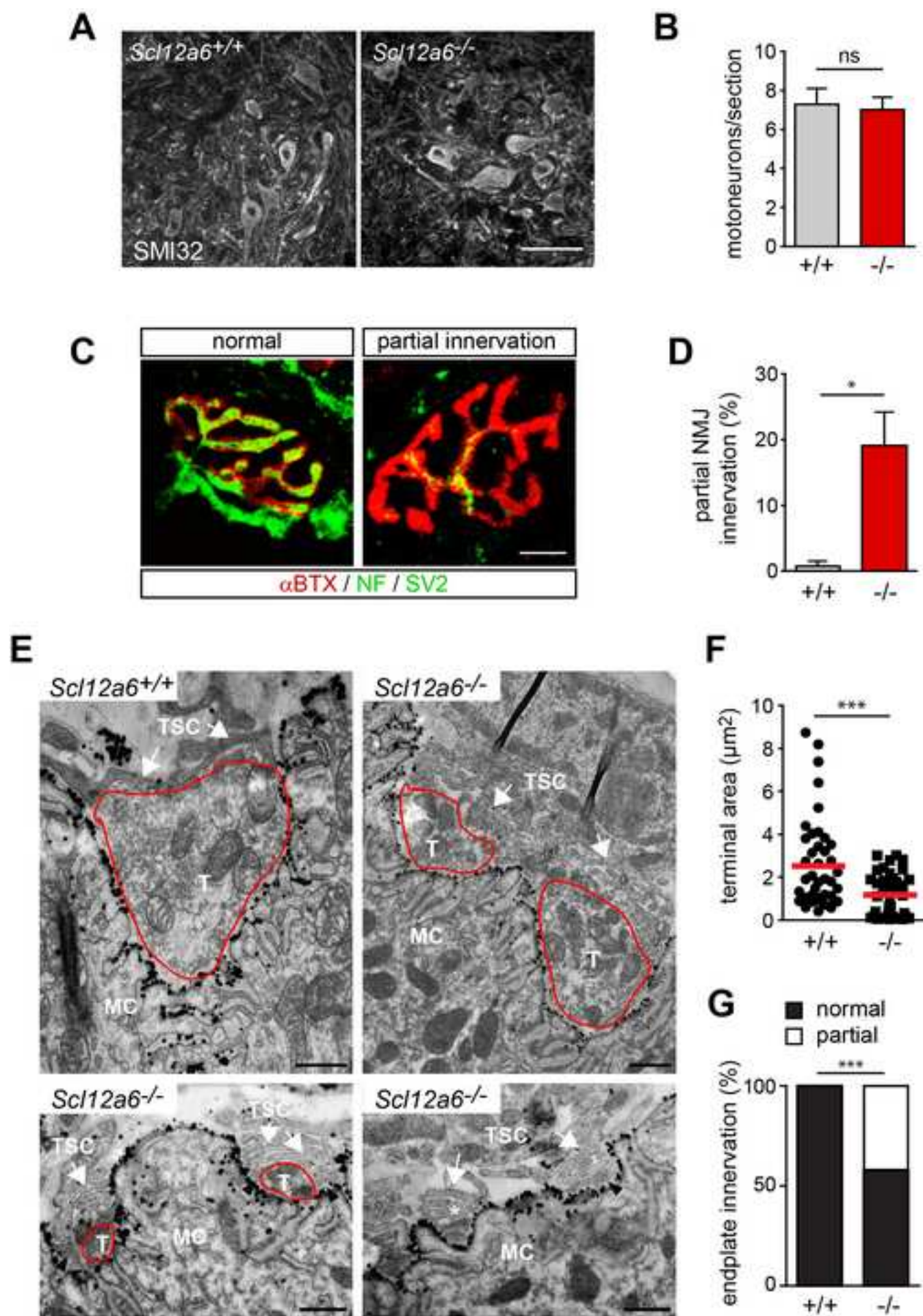


Figure 2
[Click here to download high resolution image](#)

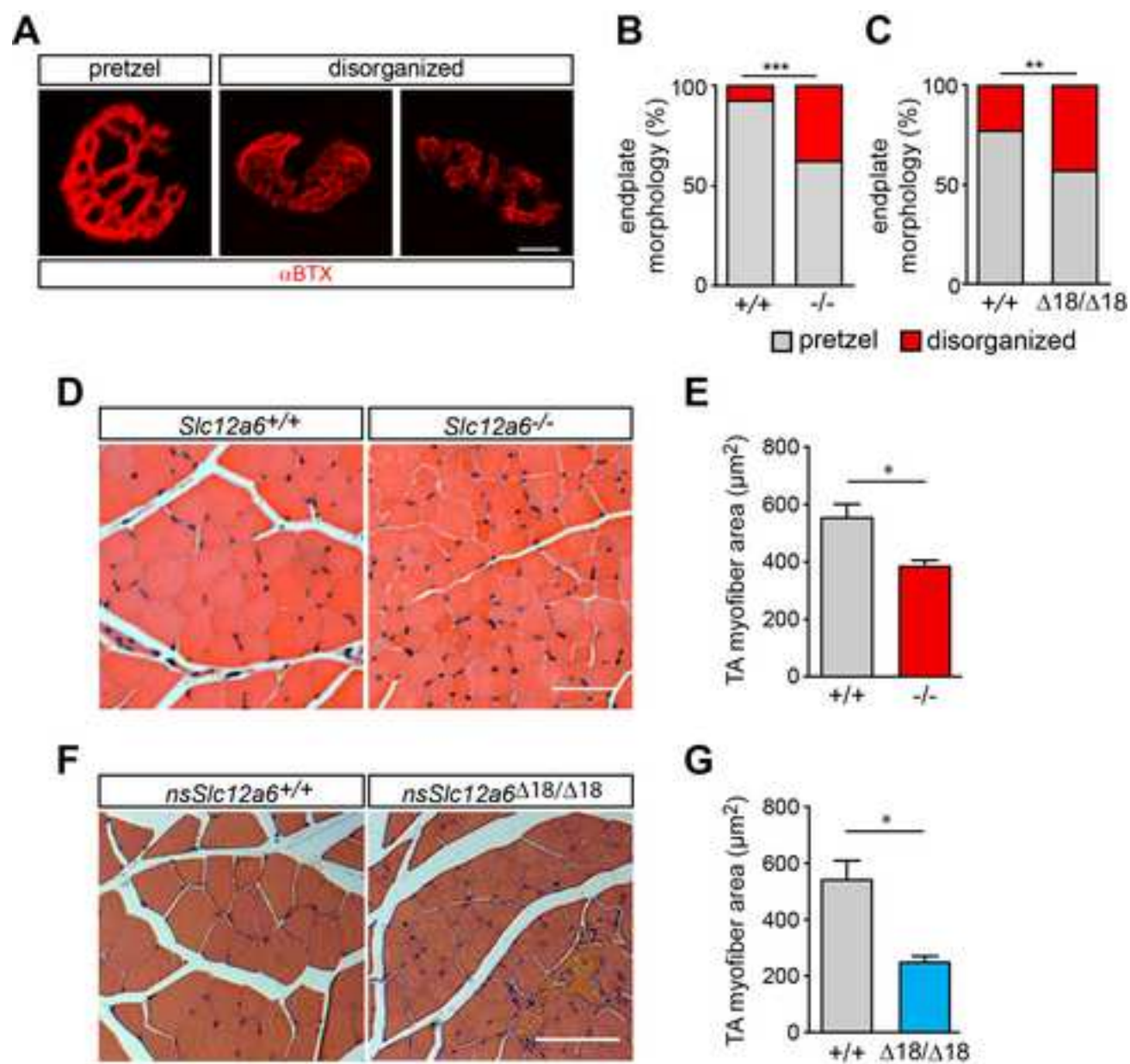
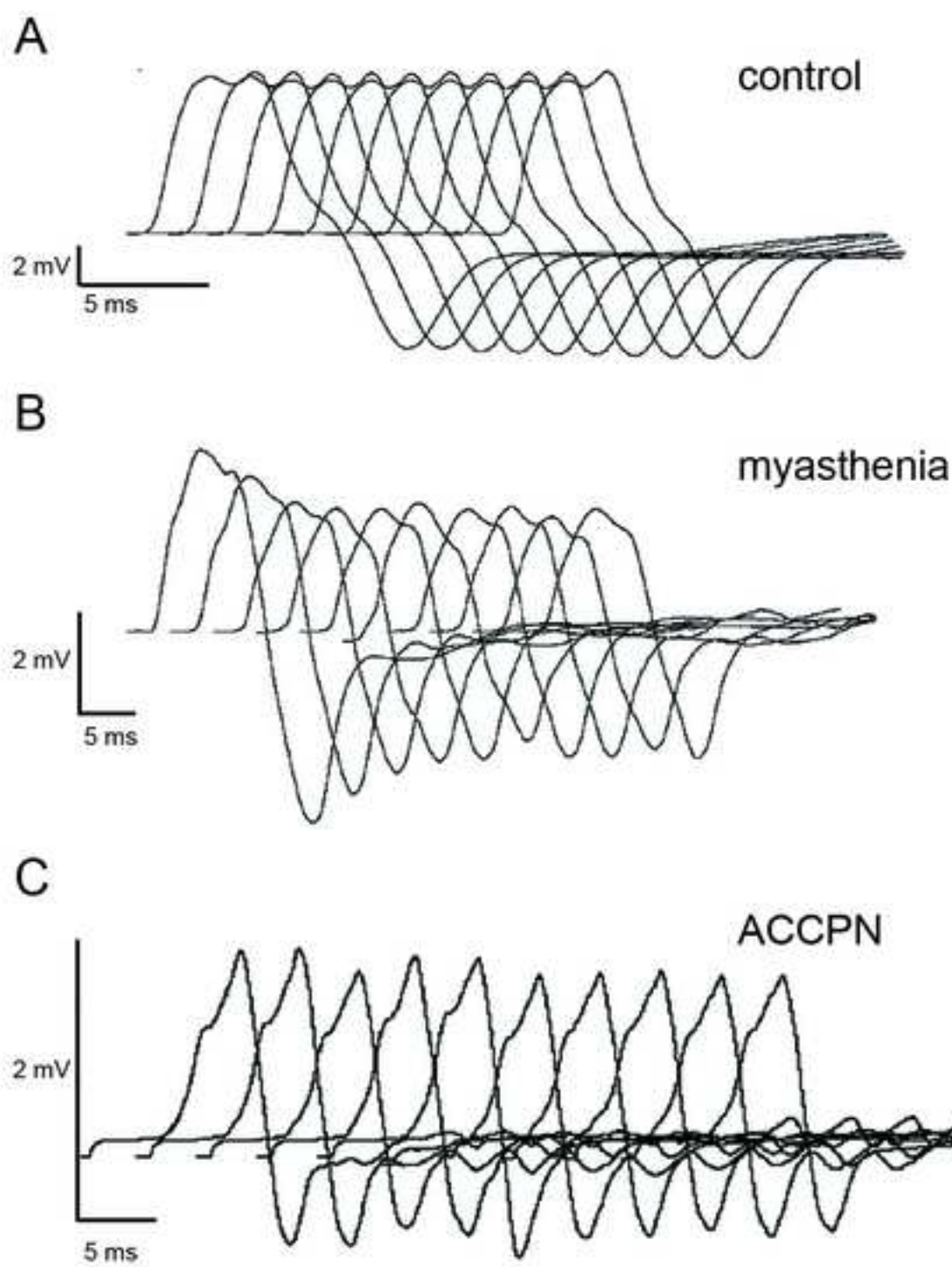


Figure 3
[Click here to download high resolution image](#)



Patient	gender	age	ACC	polyneuropathy	basal motor potential	3Hz motor potential
1	M	29	+	+	1.1 mV	1.1 mV
2	F	25	+	+	0.9 mV	0.9 mV

Figure 4
[Click here to download high resolution image](#)

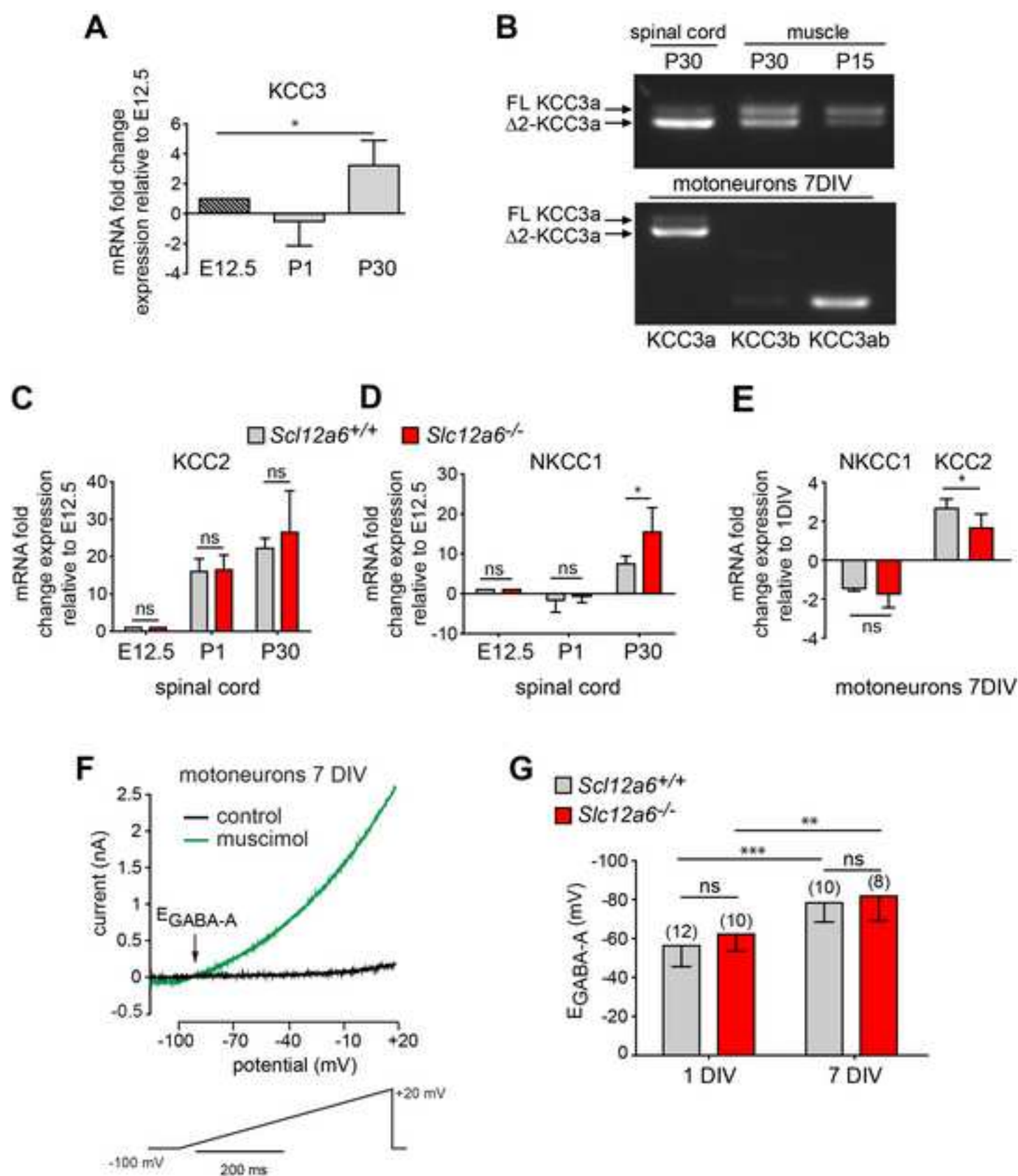


Figure 5
[Click here to download high resolution image](#)

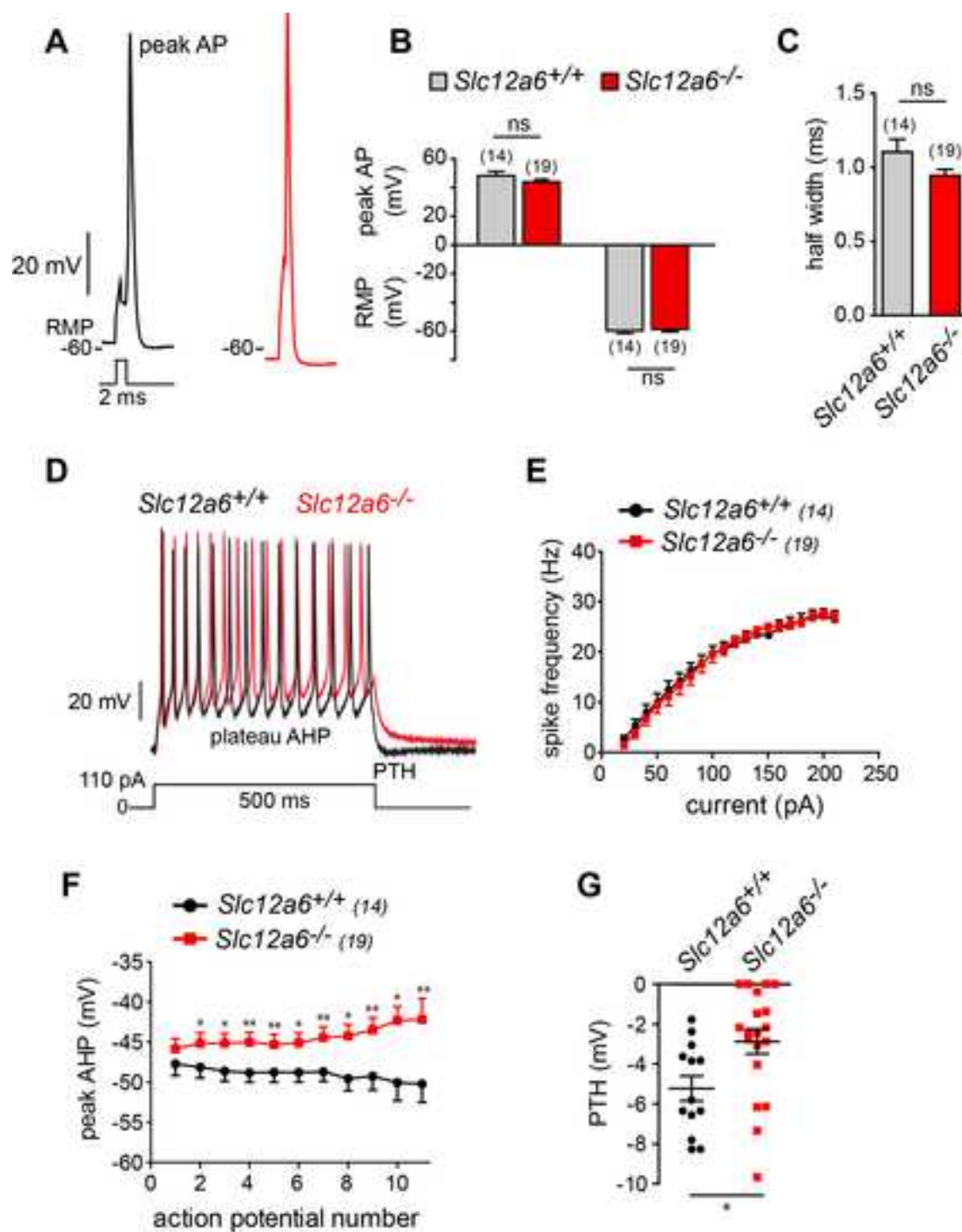


Figure 6

[Click here to download high resolution image](#)

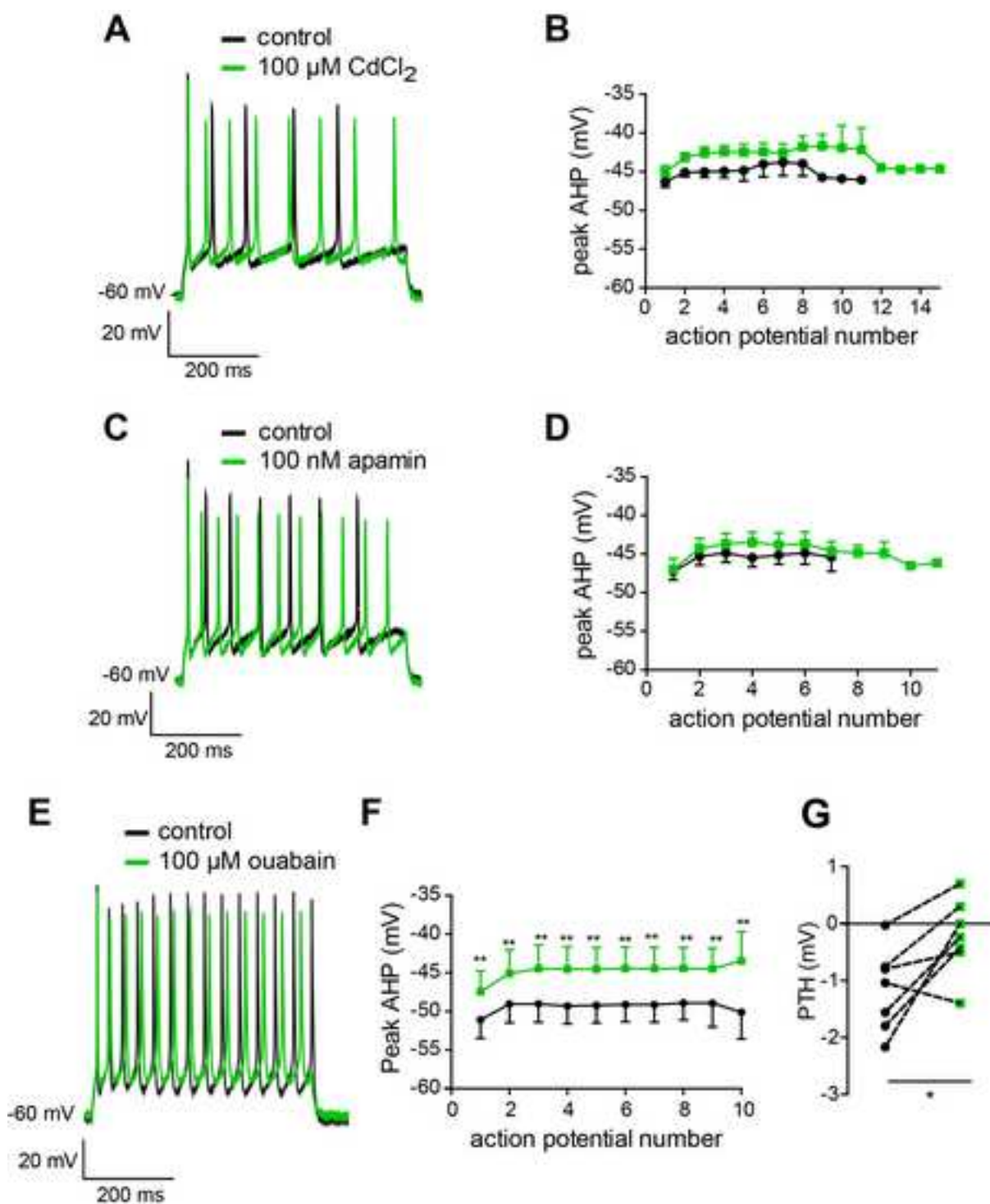


Figure 7
[Click here to download high resolution image](#)

